



ELSEVIER

A study of tungsten nanopowder formation by self-propagating high-temperature synthesis

H.H. Nersisyan ^{a,*}, J.H. Lee ^b, C.W. Won ^a

^a *Rapidly Solidified Materials Research Center, Chungnam National University, 220 Gung-Dong, Yuseong, Daejeon 305-764, Republic of Korea*

^b *Korea Atomic Energy Research Institute (KAERI), 150 Duckjin-Dong, Yuseong, Daejeon 305-353, Republic of Korea*

Received 19 August 2004; received in revised form 11 February 2005; accepted 28 March 2005

Available online 3 May 2005

Abstract

Molten salt-assisted self-propagating high-temperature synthesis of nanocrystalline W powder was studied experimentally. The technique involves the reduction of WO_3 in the presence of sodium chloride using three different reducing agents: magnesium (Mg), sodium azide (NaN_3), and sodium borohydride (NaBH_4). The effects of the mole fraction of sodium chloride on temperature distributions, combustion parameters, phase compositions, and morphology of the final products were determined. The sodium chloride-assisted method reported here has been found to be effective for lowering combustion temperature and producing uniform and spherical W nanopowders of average particle size around 20–200, 100–200, and 20–50 nm. The effect of combustion temperature on tungsten particle size is discussed, and a sketch describing the chemistry of combustion is proposed.

© 2005 The Combustion Institute. Published by Elsevier Inc. All rights reserved.

Keywords: Self-propagating high-temperature synthesis; Temperature distributions; Combustion speed; Tungsten nanopowders; Particle size; Molten salt

1. Introduction

Self-propagating high-temperature synthesis (SHS) is an attractive method for rapidly generating large quantities of materials (grams per second production rate). Compared with other powder production methods, SHS is the hottest, fastest, and most attractive scientifically, because the components interact nonisothermally when the heating rate of substances in a wave is $\sim 10^3$ to 10^6 K/s [1,2]. Exciting new

variations of traditional SHS methods are expanding the range of material systems that can be effectively produced using the combustion synthesis technique. Variations include metallothermic SHS [3], electric-field activated SHS [4], catalytically assisted SHS [5], and molten salt-assisted SHS [6].

In molten salt-assisted SHS, alkali metal halide is included as an additional reactant in the system. Alkali metal halide aids in transportation of the reactant species to reduce combustion temperature, thus producing uniform, submicrometer powders. The mutual diffusion of various atoms is much more rapid in the molten salt than in the solid state. This facilitates synthesis at low temperature, which positively affects the size of combustion products. In addition, alkali metal

* Corresponding author. Fax: +82 42 822 9401.

E-mail address: haykrasom@hotmail.com

(H.H. Nersisyan).

halide prevents grain growth by forming a protective layer around the particles.

In an earlier study, we demonstrated the effects of molten salts on the combustion parameters and material properties (particle size, composition, morphology, etc.) of the $\text{TiO}_2\text{--Mg}$ and $n\text{Ta}_2\text{O}_5\text{--Mg}$ systems [7,8]. Molten salt that was initially introduced into the reactant mixture helped to produce metal nanoparticles without any constraints. The current work complements the previous studies and describes the effect of molten salt on the combustion characteristics of the WO_3 /reducing agent system used to produce nano-sized tungsten powder. In particular, the effects of the reduction agents and alkali metal salts on combustion temperature and speed as a function of several system parameters are presented. Three reducing agents were examined: metallic magnesium, sodium azide, and sodium borohydride. Sodium chloride was selected as the main alkali metal salt based on the results of previous investigations. The results are also discussed in the context of a proposed mechanism for the reaction and relationships between combustion characteristics and material properties.

There are few alternative studies on preparing tungsten nanoparticles: a high-energy ball milling method using WO_3 and Mg as starting materials [9], plasma heating of precursor aerosol for vapor condensation [10], the gas-phase combustion synthesis method [11], sealed-tube synthesis employing WCl_6 and $\text{Si}(\text{SiMe}_3)_4$ [12]. Unlike SHS, the aforementioned techniques for tungsten nanoparticle synthesis

are generally limited in scaleup. Only small amounts are typically produced.

2. Experimental

A sketch of the experimental facility is provided in Fig. 1. Briefly, the reactant powders were thoroughly dry-mixed in a ceramic mortar and cold-stamped into a stainless-steel mold to form cylindrical specimens (3–5 cm in diameter, 4–5 cm height). The reactant properties are listed in Table 1.

Tungsten–rhenium thermocouples (W/Re-5 vs W/Re-20, 50 and 100 μm in diameter) were used to determine combustion speed (U_c) and to monitor the temperature distributions of the samples. Three thermocouple wells (3 mm in diameter, 15–20 mm deep) were drilled into each specimen perpendicular to the cylinder axis at a spacing of ~ 1 cm. The upper thermocouple was placed 1.0 to 1.5 cm from the top of the specimen. A computer at the rate of 10 Hz using a data logger (DASTC, Keithley) continuously recorded the thermocouple time histories. Combustion speeds were determined from the temperature profiles and the known spacing between the thermocouples.

All experiments were conducted in a laboratory constant-pressure reactor. At the start of the experiment, the combustion chamber was sealed, evacuated, and purged with argon. The chamber was then filled with argon to the desired partial pressure. The combustion reaction was initiated by resistively heating

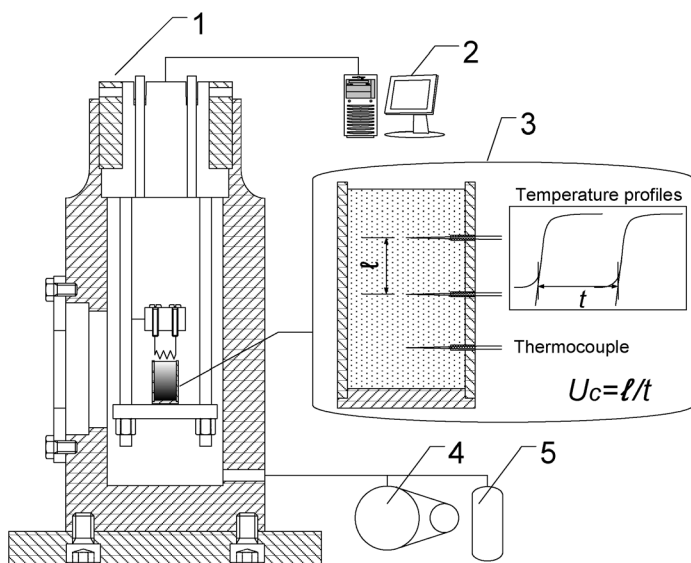


Fig. 1. Experimental schematic of the combustion chamber and the reactant specimen with thermocouples. (1) SHS reactor, (2) data logger, (3) initial sample installed with thermocouples and the definition of propagation speed, (4) vacuum pump, (5) Ar gas.

Table 1
Reactant properties

Reactant	Manufacture	Particle size (μm)	Purity (%)
Tungsten oxide	Samchun Pure Chemical, Korea	<10	98
Magnesium	Daejung Chem. and Metals, Korea	100–200	98.5
Sodium chloride	Samchun Pure Chemical, Korea	<50	99.5
Sodium azide	Samchun Pure Chemical, Korea	<50	99.5
Sodium borohydride	Acros Organics, USA	<50	98.5
Silica (quartz)	Samchun Pure Chemical, Korea	<1	99

the nickel–chromium filament. Power to the filament was immediately discontinued after ignition of the sample.

Tungsten nanopowders were characterized by using a $\text{CuK}\alpha$, Siemens D5000 X-ray diffractometer. Surface area analysis was performed on a Coulter SA3100 surface area instrument, with a BET surface area reproducibility coefficient of variation of <2%, using nitrogen gas sorption. A transmission electron microscope (JEOL 2010) was used to examine the morphology, shape, and size of the W metal nanopowders.

3. Results and discussion

Experiments were carried out using a range of mole fractions of sodium chloride and a range of reducing agents containing sodium. The experimental conditions are summarized in Table 2. Initial temperature (T_0), sample radius (r), and external pressure of argon (P_{Ar}) were kept constant at $T_0 = 298 \text{ K}$, $r = 3.0 \text{ cm}$, $P_{\text{Ar}} = 1.0$ and 2.5 MPa .

3.1. Reduction of WO_3 by Mg

A number of complete steady-state thermal profiles (from the initial cold-end temperature of the

Table 2
Experimental conditions studied in the current work

Parameter	Range
Argon pressure, MPa	1.0, 2.5
Sodium chloride mole fraction	0–7
Sodium borohydride mole fraction	0.85–2.0

specimen up to the maximum flame temperature) were collected over the salt interval from 3 to 6 mole fraction. High-pressure argon ($P_{\text{Ar}} = 2.5 \text{ MPa}$) was applied to suppress magnesium evaporation. Averaged temperature profiles of steady propagating combustion waves in the $\text{WO}_3\text{--}3\text{Mg--}k\text{NaCl}$ (here, k is the mole fraction of inert constituent) system, illustrated in Fig. 2, reveal single-stage (at $k = 4.0$) and multistage (at $k = 5.0, 5.5$) temperature distributions resulting from the melting and boiling of reactants. Here T^* is the starting temperature of the chemical reaction and agrees with the melting point of magnesium (650°C). The ordinate flame structure is separated into two zones: the so-called preflame zone (left side) and the chemical conversion zone (right side). With $k = 4$, in the beginning of the reaction zone, the temperature increases rapidly to $1400\text{--}1450^\circ\text{C}$ and then the long tail of the afterburning zone follows. The nearly isothermal areas at 600, 800, and

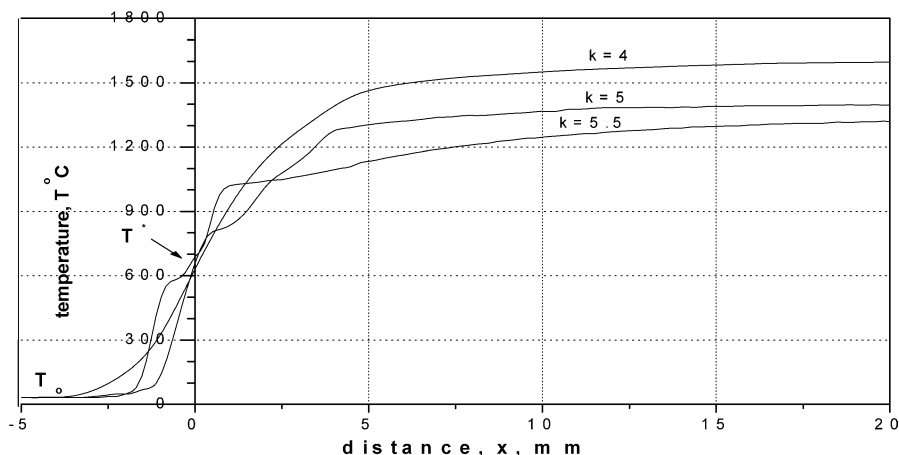


Fig. 2. Experimental profiles of temperature versus NaCl mole fraction.

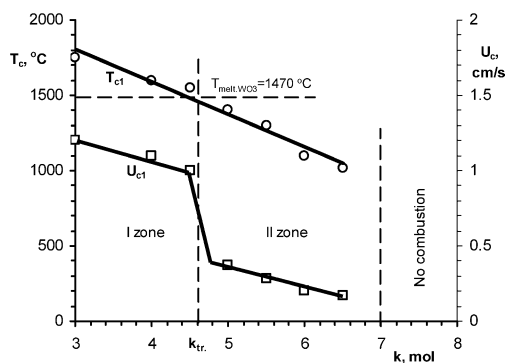


Fig. 3. Effect of NaCl mole fraction on combustion temperature and speed.

1000–1100 °C registered at $k = 5$ and 5.5 seem to be related to the heat consumed in the melting and evaporation of Mg and the melting of NaCl. These zones are not easily detectable because of the blocking effect of the combustion temperature.

Plots of the combustion parameters of the $\text{WO}_3 + 3\text{Mg} + k\text{NaCl}$ system against k are shown in Fig. 3. Combustion temperature (T_c) decreases linearly from 1750 to 1020 °C when k increases. In contrast to T_c , the transition point was found for U_c at $k_{tr} = 4.6$. The temperature is 1470 °C at this point, which agrees with the melting point of WO_3 . About four-fold change of combustion speed takes place at the transition from zone 1 to zone 2. The observed character of U_c is conditioned by melting of WO_3 that results in homogeneous liquid phase formation. Consequently, diffusion rate leads to more rapid transport by liquid-phase agents which results in higher combustion speeds.

The results of the study were also examined in the context of the phase composition final products obtained. XRD investigation revealed that a spasmodic change in combustion speed does not affect the final product composition; that is, phase pure W after cleaning from MgO and NaCl (Figs. 4a and 4b). Near to the combustion limit (at $k = 6$), when temperature is too low (≤ 1100 °C), along with elemental tungsten combustion reaction produces MgWO_4 as a by-product (Fig. 4c).

3.2. Reduction of WO_3 using sodium compounds

The low dissociation temperatures of the sodium compounds used ($T_{dis.}(\text{NaN}_3) = 275$ °C, $T_{dis.}(\text{NaBH}_4) = 400$ °C [13]) make them attractive reducing agents for reducing flame temperature because elemental sodium and sodium boride are expected to form in the preflame zone. Powder mixtures of $\text{WO}_3 + 6\text{NaN}_3 + 3\text{SiO}_2 + k\text{NaCl}$ and $\text{WO}_3 + \alpha\text{NaBH}_4 + \text{NaCl}$ composition were used in the combustion experiments.

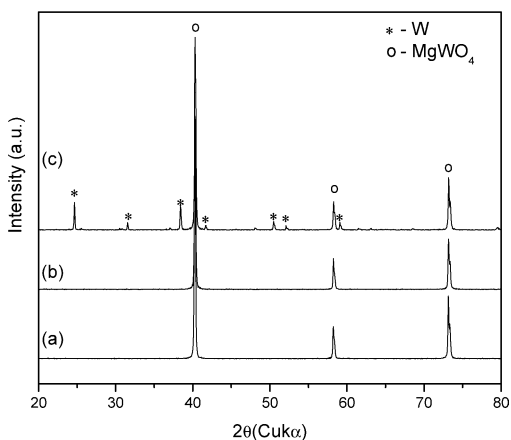


Fig. 4. X-ray patterns of the powders at different k : (a) 3.0, (b) 4.0, (c) 6.0.

In Fig. 5 are the thermal profiles of the combustion waves of the $\text{WO}_3 + 6\text{NaN}_3 + 3\text{SiO}_2 + k\text{NaCl}$ (Fig. 5a) and $\text{WO}_3 + \alpha\text{NaBH}_4 + \text{NaCl}$ (Fig. 5b) systems. Basically, they are single stages in which quantitative effects are small, because of the high propagation speed and the blocking effect of the combustion temperature. It can be seen from the given results that the sodium azide reduction process has a lower starting temperature ($T^* = 300$ °C) than the sodium borohydride reduction process ($T^* = 450$ °C). These temperatures agree with the dissociation temperatures of the sodium compounds used.

The results of the temperature and speed measurements on combustion of the $\text{WO}_3 + 6\text{NaN}_3 + 3\text{SiO}_2 + k\text{NaCl}$ mixture are illustrated in Fig. 6. It can be seen that combustion temperature decreases linearly from 1180 to 830 °C as k increases from 0 to 7. At $k > 7$, attenuation of the combustion process occurs. Note that combustion temperatures higher than the melting point of NaCl (810 °C) are obtained. Wave propagation speed is similar to with respect to the tendency temperature to decrease. The values for speed are high for the given temperatures due to liquid sodium formation in the preflame zone. XRD patterns of the powder as received and washed with deionized water are shown in Fig. 7. Two phases were observed after combustion: tungsten and sodium silicate– Na_2SiO_3 (Fig. 7a). Phase pure tungsten powder was obtained after purification of reaction products with deionized water (Fig. 7b). Note that no influence of combustion temperature on the phase composition of the final product over the interval 1180–900 °C ($0 \leq k \leq 5$) was observed. Meanwhile, partial formation of tungsten nitride (W_2N) occurs at $T < 900$ °C, and rapidly increases with decreasing temperature.

The reduction of WO_3 by means of NaBH_4 proceeds at lower temperatures as follows from the re-

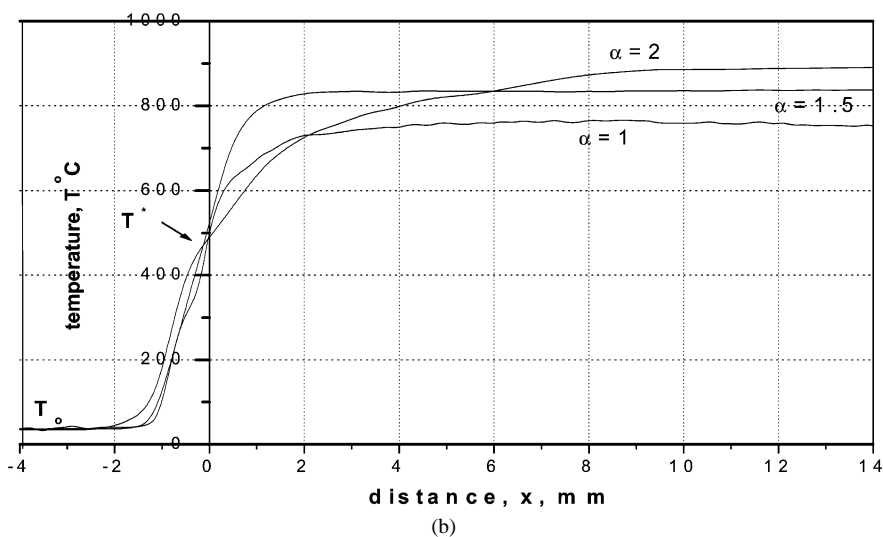
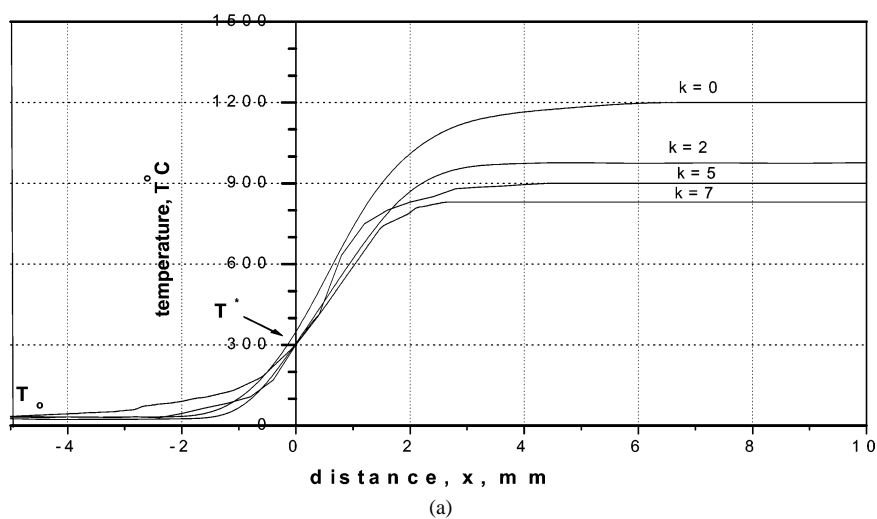


Fig. 5. Experimental thermal profiles of the $\text{WO}_3 + 6\text{NaN}_3 + 3\text{SiO}_2 + k\text{NaCl}$ (a) and $\text{WO}_3 + \alpha\text{NaBH}_4$ (b) systems.

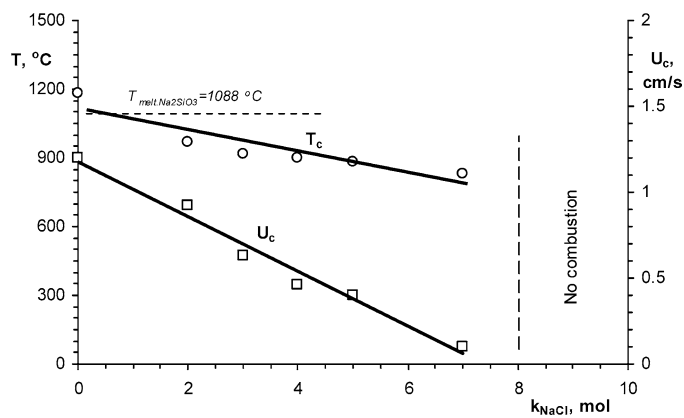


Fig. 6. Combustion temperature and speed versus NaCl mole fraction.

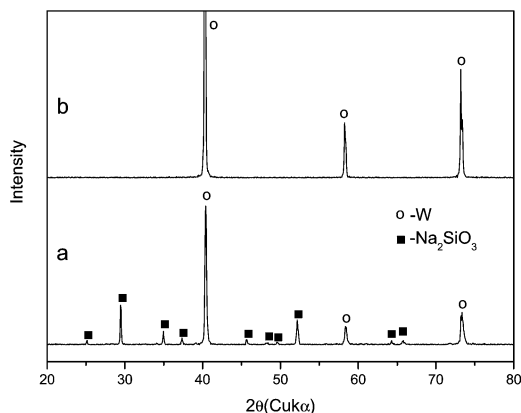


Fig. 7. X-ray diffraction patterns of the combustion products: (a) as obtained, (b) washed with deionized water.

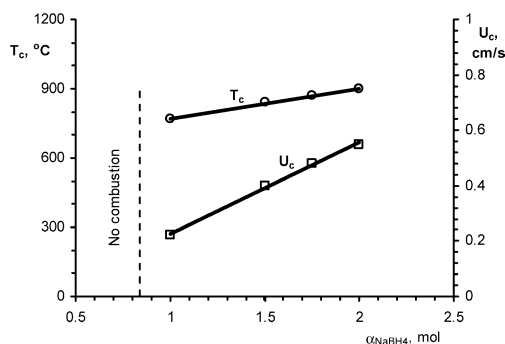


Fig. 8. Combustion temperature and speed versus NaBH_4 mole fraction.

results illustrated in Fig. 8. Here, the mole fraction of NaBH_4 (α) was varied in view of the actual stoichiometry of reactants, which corresponds to $\alpha = 1.5$. The results imply that maximum values of the combustion parameters do not agree with the stoichiometric point, which most likely is the result of different chemical processes proceeding in the combustion wave. This is confirmed by the results of X-ray investigation shown in Fig. 9. Multiple phase structures with substantial amounts of complex tungsten oxides (Na_2WO_4 and NaWO_3) were recorded at $\alpha = 1.0$ (Fig. 9a). With an increase in α , the amount of NaWO_3 decreases (Fig. 9b) and becomes practically zero at the stoichiometric point ($\alpha = 1.5$). However, there is still plenty of Na_2WO_4 (about 10%) in the final product at this point (Fig. 9c). Complete reduction of WO_3 occurs at $\alpha = 2.0$, when combustion temperature is maximum (900°C). XRD detected no perceptible amount of NaBO_2 , which forms during the combustion as a main by-product of NaBH_4 oxidation. Single-phase tungsten was obtained after washing of the final products, as NaBO_2 and Na_2WO_4 are easily soluble in water (Fig. 9d).

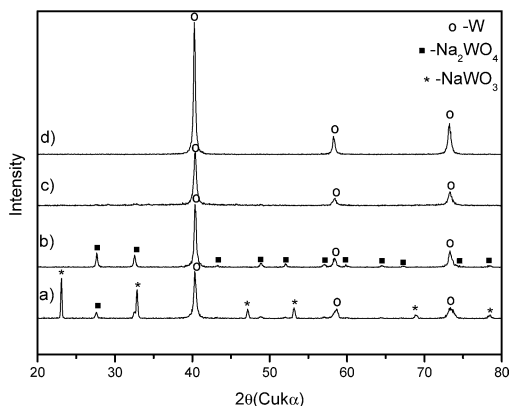


Fig. 9. X-ray patterns of the products obtained at different α : (a) 1.0, (b) 1.5, (c) 2.0, (d) 1.5 (washed powder).

The results obtained clearly indicate the essential role of temperature in phase formation processes during the synthesis of tungsten powder.

In addition to successful synthesis of a single-phase powder of elemental tungsten, the XRD patterns yield an estimate of normal particle size from the Scherrer equation ($r = 0.89\lambda / \beta \cos \theta$). Here, r is crystallite thickness, λ is X-ray wavelength, β is the full width at half-maximum (FWHM) of the peak, and θ is the angle at FWHM. Comparison of the XRD peaks of W powders (Figs. 4, 7, 9) shows that the tungsten powder obtained by means of NaBH_4 has mostly broad peaks, thus indicating nanodimensions. The size of particles calculated with the Scherrer equation corresponds to 50 nm.

3.3. Morphology and size distributions of W powders

TEM images of W nanoparticles produced by different reducing agents are shown in Fig. 10. It can be seen that polydispersed and spherical W particles were formed during the reduction of WO_3 by Mg (Fig. 10a). Most of the particles are smaller than 100 nm; however, some of them are about 100–200 nm. We suppose that the formation of large particles is caused by the consolidation of smaller ones because of high combustion temperature (1600°C) and unsatisfactory protection by molten salt. The tungsten powder prepared by the NaN_3 method at 1000°C has a more uniform size distribution ranging from 100 to 200 nm (Fig. 10b). The fraction of particles below 100 nm is noticeably lower in comparison with that obtained by the Mg reduction method. In contrast to the other cases, the NaBH_4 reduction method produces very uniform and spherical W particles at 800°C ranging in size from 20 to 50 nm (Fig. 10c).

To estimate the specific surface areas of the tungsten powders produced, the appropriate BET analysis

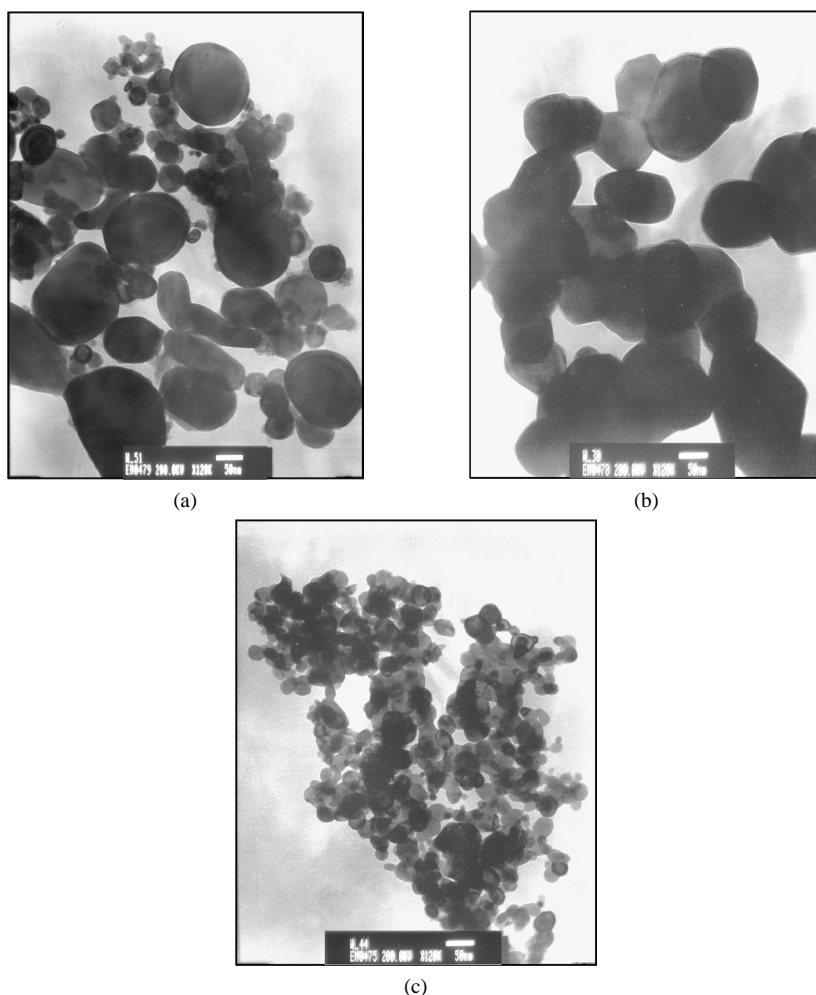


Fig. 10. TEM images of the W nanoparticles prepared: (a) Mg reduction method, (b) NaN_3 reduction method, (c) NaBH_4 reduction method.

Table 3
Results of BET and TEM analyses of the W powders

Initial mixture	Gas	Specific surface area (m^2/g)	Average particle size (nm)
$\text{WO}_3 + 3\text{Mg} + 4\text{NaCl}$	Nitrogen	5.9	20–200
$\text{WO}_3 + 6\text{NaN}_3 + 3\text{SiO}_2$	Nitrogen	4	100–200
$\text{WO}_3 + 1.5\text{NaBH}_4 + \text{NaCl}$	Nitrogen	12	20–50

was conducted. Average particle sizes estimated from the micrographs and values of specific surface area analyzed by BET are listed in Table 3.

3.4. The mechanism of the combustion and tungsten nanoparticle formation

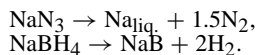
The results obtained in this study indicate that the proposed method is novel and effective in produc-

ing W nanopowders under the combustion mode. Two factors responsible for W nanoparticle formation can be noted: low combustion temperature and high mole fraction of alkali metal salt. When the salt fraction is high, combustion temperature and wave propagation speed are low; the molten salt has time to form strong protective layers around primary tungsten particles, thus maintaining their nanostructure. At higher temperature, the mobility of molten salt is high and the protective effect reverses, so grain growth occurs

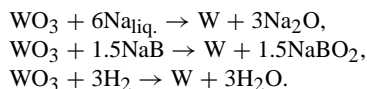
during combustion. That is why the Mg and NaN_3 reduction methods produce relatively larger particles than the NaBH_4 reduction method. A distinguishing feature of sodium salt reduction methods is the formation of a number of sodium compounds (Na_2O , Na_2SiO_3 , NaBO_2 , and Na_2WO_4) which have low melting points and can inhibit grain growth. The temperature range 850–1000 °C is optimum for synthesis of W nanoparticles by the given technique.

Reaction pathway analysis shows that the reduction of WO_3 by sodium-containing reducing agents is a complex physicochemical process consisting of many elemental acts that proceed in different reaction zones (pre flame, combustion, and afterburning). These zonal reactions mechanisms are given below:

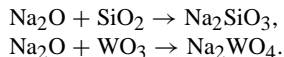
1. *Pre flame zone*: Decomposition of sodium salt in this zone occurs due to reaction heat:



2. *Combustion zone*: In this zone formation of W occurs. After sodium compounds decompose, WO_3 reduction becomes easier:



3. *Afterburning zone*: New sodium containing salts form in this zone:



4. Conclusions

The combustion wave parameters (T_c , U_c) and temperature distributions of the WO_3 –reducing agent (Mg, NaN_3 , NaBH_4)–NaCl mixture, using controlled amounts of sodium chloride, were experimentally obtained. Comparison with pure mixture parameters

(without sodium chloride) indicates that a significant decrease in values occurs when sodium chloride is added because of the heat required to warm up, latent heat, and liquid-phase NaCl melt. Molten sodium chloride in combination with low combustion temperature acts as a protective medium against grain growth of the tungsten obtained. As a result, nanosize tungsten powders with different size distributions are obtained.

Current and future works include improved modeling efforts to describe molten salt-assisted SHS systems, SHS chemistry, and diffusion process evaluation in molten salt-assisted systems, where the reactants and products undergo phase changes leading to the formation of nanostructured material.

References

- [1] A.G. Merzhanov, Int. J. SHS 4 (1995) 323.
- [2] Z.A. Munir, U. Anselmi-Tamburini, Mater. Sci. Rep. 69 (1989) 277.
- [3] A.G. Merzhanov, J. Mater. Proc. Technol. 56 (1996) 222–241.
- [4] H. Xue, Z.A. Munir, Int. J. SHS 5 (1996) 229–237.
- [5] L. Wang, M.R. Wixom, L.T. Tompson, J. Mater. Sci. 26 (1990) 534–544.
- [6] H.H. Nersisyan, J.H. Lee, C.W. Won, J. Mater. Res. 17 (2002) 2859–2864.
- [7] H.H. Nersisyan, J.H. Lee, S.I. Lee, C.W. Won, Combust. Flame 135 (2003) 539–545.
- [8] H.H. Nersisyan, J.H. Lee, C.W. Won, Mater. Res. Bull. 38 (2003) 1135–1146.
- [9] R. Ricceri, P. Matteazzi, J. Alloys Compd. 358 (1/2) (2003) 71–75.
- [10] J. Phillips, W.L. Perry, U.S. Patent 6689192 (2004).
- [11] R.L. Axelbaum, J.I. Huertas, C.R. Lottes, S. Hariprasad, S.M.L. Sastry, Mater. Manufacturing Processes 11 (1996) 1043–1053.
- [12] Y.H. Chang, H.S. Wang, C.H. Chiu, D.S. Cheng, M.Y. Yen, H.S. Chiu, Chem. Mater. 14 (2002) 4334–4338.
- [13] R.C. Weast, Handbook of Chemistry and Physics, CRC Press, Boca Raton, FL, 1987–1988.